Oxidized Cholesterol Metabolites Found in Human Atherosclerotic Lesions Promote Apolipoprotein C-II Amyloid Fibril Formation †

ARTICLE *in* BIOCHEMISTRY · JUNE 2007

Impact Factor: 3.02 · DOI: 10.1021/bi602554z · Source: PubMed

Oxidized Cholesterol Metabolites Found in Human Atherosclerotic Lesions Promote Apolipoprotein C-II Amyloid Fibril Formation†

Cameron R. Stewart,‡,§ Leanne M. Wilson,‡,§ Qinghai Zhang,‡,|| Chi L. L. Pham,§ Lynne J. Waddington,⊥ Maree K. Staples,§ David Stapleton,§ Jeffery W. Kelly,|| and Geoffrey J. Howlett*,§

Department of Biochemistry and Molecular Biology, Bio21 Molecular Science and Biotechnology Institute, The University of Melbourne, Parkville, Victoria 3010, Australia, Department of Chemistry and The Skaggs Institute of Chemical Biology, The Scripps Research Institute, La Jolla, California 92037, and Commonwealth Scientific and Industrial Research Organisation, Parkville, Victoria 3052, Australia

Received December 12, 2006; Revised Manuscript Received March 9, 2007

ABSTRACT: Apolipoprotein amyloid deposits and lipid oxidation products are colocalized in human atherosclerotic tissue. In this study we show that the primary ozonolysis product of cholesterol, 3β-hydroxy-5-oxo-5,6-secocholestan-6-al (KA), rapidly promotes human apolipoprotein (apo) C-II amyloid fibril formation in vitro. Previous studies show that hydrophobic aldehydes, including KA, modify proteins by the formation of a Schiff base with the lysine ϵ-amino group or N-terminal amino group. High-performance liquid chromatography, mass spectrometry, and proteolysis of KA-modified apoC-II revealed that KA randomly modified six different lysine residues, with primarily one KA attached per apoC-II molecule. Competition experiments showed that an aldehyde scavenging compound partially inhibited the ability of KA to hasten apoC-II fibril formation. Conversely, the acid derivative of KA, lacking the ability to form a Schiff base, accelerated apoC-II fibril formation, albeit to a lesser extent, suggesting that amyloidogenesis triggered by KA involves both covalent and noncovalent mechanisms. The viability of a noncovalent mechanism mediated by KA has been observed previously with α-synuclein aggregation, implicated in Parkinson's disease. Electron microscopy demonstrated that fibrils formed in the presence of KA had a similar morphology to native fibrils; however, the isolated KA−apoC-II covalent adducts in the absence of unmodified apoC-II formed fibrillar structures with altered ropelike morphologies. KA-mediated fibril formation by apoC-II was inhibited by the addition of the amine-containing compound hydralazine and the lipid-binding protein apoA-I. These in vitro studies suggest that the oxidized small molecule pool could trigger or hasten the aggregation of apoC-II to form amyloid deposits.

Atherosclerosis is a vascular disease characterized by the accumulation of lipids and proteins in the walls of medium- and large-sized arteries (*1*). The disease is also associated with chronic inflammation, attributed, at least in part, to oxidative damage within the artery wall (*2*). High levels of oxidative stress are linked to elevated levels of oxidized lipids and the generation of an oxidized small molecule pool (*3*). Ozone, one of the most reactive oxidants known, has recently been identified as one of the oxidants present in human atherosclerotic arteries (*4*). The proposed mechanism of ozone formation is via the antibody-catalyzed water oxidation pathway (*5*). Several products of cholesterol ozonolysis have been detected in human atherosclerotic tissue (*4*) where the principle product is a keto aldehyde derivative, 3β-hydroxy-5-oxo-5,6-secocholestan-6-al, also known as atheronal A. This compound and its aldolization product (atheronal B) form an equilibrium mixture referred to here as KA.[1] This mixture has been shown to deform low-density lipoproteins (LDL), to increase LDL uptake by macrophages, and to be cytotoxic to a range of cells found within atheroma (*4*), suggesting KA may contribute to disease development.

Amyloid fibril deposition is one of the defining features of Alzheimer's, Parkinson's, and related amyloid diseases. Aβ amyloid fibrils derived from Alzheimer plaques promote a range of proinflammatory effects in macrophages and brain microglia including stimulation of the production of chemokines, cytokines, and reactive oxygen species (*6, 7*). KA promotes amyloidogenesis of the Aβ (1−40) peptide by a covalent mechanism (*8, 9*). KA, found at elevated levels in Lewy body dementia cortices, also accelerates α-synuclein aggregation, implicated in Parkinson's disease, by what appears to be a noncovalent mechanism (*10*).

Recent studies demonstrate that amyloid deposits are present in up to 50−60% of aortic atherosclerotic lesions

† This work was supported by Australian Research Council Grant DP0449510 and National Health and Medical Research Council Grant 208913 to G.J.H. and by NIH Grant NS 50636 to J.W.K.

* Corresponding author. Phone: 61 3 8344 2271. Fax: 61 3 9347 7730. E-mail: ghowlett@unimelb.edu.au.

‡ These authors contributed equally.

§ The University of Melbourne.

|| The Scripps Research Institute.

⊥ Commonwealth Scientific and Industrial Research Organisation.

[1] Abbreviations: 4-HNE, 4-hydroxy-2*E*-nonenal; 9-ONC, 9-oxononanoylcholesterol; Aβ, β-amyloid; apo, apolipoprotein; BSA, bovine serum albumin; CD, circular dichroism; HPLC, high-performance liquid chromatography; KA, 3β-hydroxy-5-oxo-5,6-secocholestan-6-al; LDL, low-density lipoproteins; MALDI, matrix-assisted lazer desorption ionization; MRE, mean residue ellipticity; MS, mass spectrometry; ThT, thioflavin T; TOF, time of flight.

10.1021/bi602554z CCC: $37.00
Published on Web 04/13/2007

(*11*−*13*). Prominent among the list of amyloid proteins identified in atherosclerotic lesions are several members of the plasma apolipoproteins, including apoA-I, apoB, apoC-II, and apoE (*14*, *15*). Although usually associated with lipoprotein particles, apoC-II is also secreted by macrophages and is detected in both human (*15*) and mouse atheroma (*16*) where it colocalizes with serum amyloid P, a universal constituent of human amyloid deposits (*15*). These data provide indirect evidence that apoC-II forms amyloid fibrils in vivo. However, definitive evidence for the presence of apoC-II fibrils in vivo requires the development of specific reagents that can distinguish fibrillar and nonfibrillar forms of this protein.

Amyloid fibrils formed by apolipoprotein (apo) C-II have been extensively characterized in vitro, and these studies provide the basis for much of the current knowledge of amyloid fibril formation by apolipoproteins (*17*). ApoC-II is a 79 amino acid protein which activates lipoprotein lipase and adopts a primarily α-helical structure in the presence of lipid (*18*). In the absence of lipid, apoC-II has limited conformational stability and readily forms twisted ribbon-like fibrils, with all of the hallmarks of amyloid, including the induction of thioflavin T (ThT) fluorescence (*19*). We have recently shown that α1 antichymotrypsin, a component of amyloid deposits in Alzheimer's disease, accelerates fibril formation by apoC-II (*20*) and that SAP induces apoC-II fibril tangling (*21*). Hydrogen/deuterium exchange and proteolysis experiments identify a core region near the C-terminus of apoC-II that retains the ability to form amyloid fibrils (*22*). Similar regions have also been identified by computational predictions in apoA-I and apoA-II (*23*). Similar to fibrils formed by the Aβ peptide, apoC-II fibrils initiate macrophage inflammatory responses via the CD36 scavenger receptor, including increased reactive oxygen species production and TNF-α expression (*15*).

The findings that ozone oxidation products of cholesterol can significantly hasten the amyloidogenesis rate of Aβ and α-synuclein prompted the present investigation of the effect of lipid oxidation products on the rate of amyloidogenesis and conformational changes within human apoC-II. Interestingly, the distinct mechanisms by which KA hastens Aβ and α-synuclein amyloidogenesis both seem to operate in the case of metabolite-triggered apoC-II amyloidogenesis.

EXPERIMENTAL PROCEDURES

Materials. ApoC-II was expressed and purified as described previously (*16*) and stored as a stock in 5 M GuHCl at a concentration of 26.1 mg/mL. 4-Hydroxy-2*E*-nonenal (4-HNE) was stored in ethanol (64 mM) as purchased from Cayman Chemical Co. (Ann Arbor, MI). Cholesterol derivatives, including 9-oxononanoylcholesterol (9-ONC), 3β-hydroxy-5-oxo-5,6-secocholestan-6-al (KA), and 3β,6-hydroxy-5-oxo-5,6-secocholestane (keto alcohol) and its keto acid derivative, were prepared as described elsewhere (*4*, *9*, *10*, *24*) and stored in isopropyl alcohol (10 mM) at −80 °C before use. L-Carnosine, hydralazine, lysine, bovine serum albumin (BSA), and human apoA-I were purchased from Sigma (Castle Hill, NSW, Australia).

Thioflavin T Fluorescence. ApoC-II amyloid fibrils were formed by direct dilution of apoC-II stock solution into refolding buffer (100 mM sodium phosphate buffer, pH 7.4) without stirring at 20 or 37 °C. ThT fluorescence of samples (25 μL aliquots) was determined using 8 μM ThT in refolding buffer (final volume 250 μL) in an f_{max} plate reader (Molecular Devices, Sunnyvale, CA) equipped with 444/485 nm excitation/emission filters. Data were corrected for the small effect of KA alone on ThT fluorescence values. ThT time courses were analyzed to obtain the time required for half-maximal change using a three-parameter Hill plot (*25*).

Circular Dichroism Spectroscopy. Circular dichroism (CD) spectra were recorded in a model 62DS AVIV CD spectrometer at 20 °C. The spectra were measured in 1 mm quartz cuvettes, and data were collected from 250 to 200 nm at 0.5 nm intervals with a bandwidth of 1.5 nm. The mean residue ellipticity (MRE) was calculated from the equation MRE = $\theta/(cnl/M)$, where l is the path length in millimeters, θ is the observed ellipticity in millidegrees, c is the concentration of protein (mg/mL), n is number of amino acid residues, and M is the molecular weight. Spectra were corrected for baseline using the spectrum for buffer alone.

Sedimentation Velocity Analysis. Samples were analyzed at 20 °C using an XL-A analytical ultracentrifuge (Beckman Coulter, Fullerton, CA) equipped with an AnTi60 rotor. Samples (360 μL) were added to double-sector epon-filled centerpieces, with refolding buffer in the reference compartment. Radial absorbance data were acquired in the continuous scanning mode over 10 min intervals at 280 nm with radial increments of 0.002 cm and a rotor speed of 8000 rpm. The radial profiles were fitted to a model describing the sedimentation of a distribution of sedimentation coefficients with no diffusion [ls-g*(s)] assuming a time-independent background using SEDFIT (*26*).

Electron Microscopy. ApoC-II fibrils were applied to freshly glow-discharged carbon-coated copper grids and negatively stained with 2% (w/v) potassium phosphotungstate, pH 6.8. Samples were examined using a FEI Tecnai 12 transmission electron microscope equipped with a Soft Imaging System MegaView III CCD camera. Micrographs were recorded at nominal magnifications of 150000×.

Competition Experiments. ApoC-II fibrils (42 μM) were formed as described above in the presence and absence of 20 μM KA with and without 100 μM L-carnosine and 100 μM hydralazine. In addition, apoC-II fibrils (42 μM) were formed in the presence and absence of 60 μM KA with or without 100 μM lysine, 100 μM bovine serum albumin (BSA), or 10 μM apoA-I. Samples were incubated at 20 °C for 7 h before ThT fluorescence measurements.

High-Performance Liquid Chromatography. Procedures for the purification of GluC peptides derived from apoC-II were similar to those described previously (*22*). Freshly prepared apoC-II (42 μM) was incubated for 3 h in the absence and presence of KA. Samples were then reduced by the addition of 8.2 mM sodium borohydride for 30 min and analyzed by high-performance liquid chromatography (HPLC) using a Spectroflow HPLC system (Applied Biosystems, Foster City, CA) with a 10 × 250 mm C4 column (Perkin-Elmer, Boston, MA) using a solvent flow rate of 3 mL/min. Samples were eluted using solvent A [0.1% trifluoroacetic acid (TFA)] and a linear gradient of 0−90% solvent B (100% acetonitrile) over a period of 50 min. Separation was monitored by absorbance at 214 nm. Samples were analyzed either immediately or after digestion by

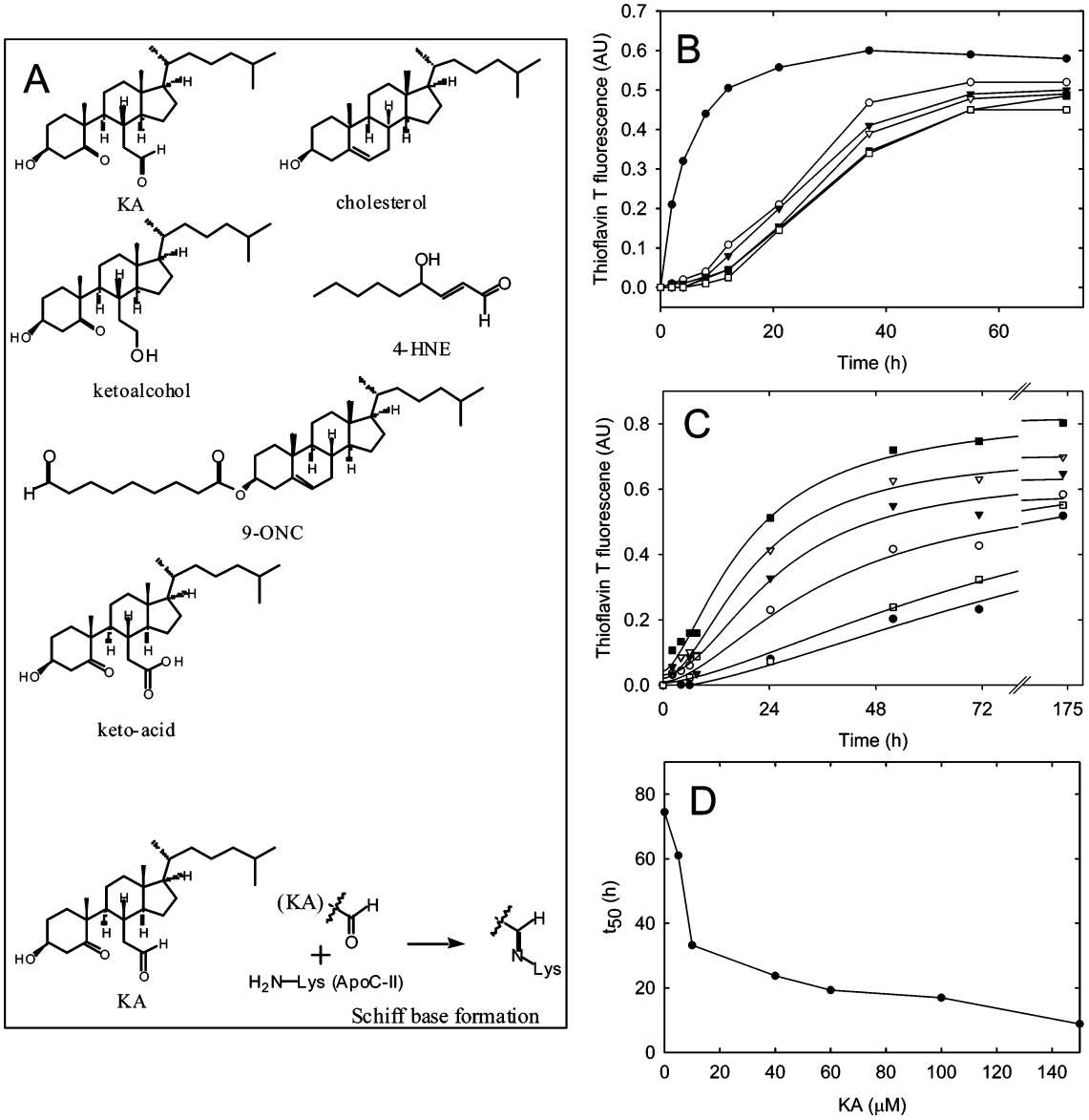

FIGURE 1: Effect of lipid metabolites on apoC-II amyloid fibril formation, monitored by ThT fluorescence. (A) Chemical structures of KA and other derivatives used in this study. (B) ApoC-II (42 μM) was incubated alone (open squares) or in the presence of 60 μM KA (closed circles) without stirring. ApoC-II was also incubated with 60 μM cholesterol (closed triangles), 60 μM 4-HNE (open triangles), 60 μM keto alcohol (closed squares), and 60 μM 9-ONC (open circles). The experiments were performed at 37 °C to facilitate the complete fibril formation of apoC-II in 3 days. (C) Concentration-dependent effect of KA on apoC-II amyloid formation. ApoC-II at 42 μM was incubated alone (closed circles) and with KA at concentrations of 5 μM (open squares), 10 μM (open circles), 40 μM (closed triangles), 60 μM (open triangles), and 100 μM (closed squares) at 20 °C. (D) Values of t_{50} (time to reach half-maximum change) for apoC-II fibril formation observed in (C) as a function of KA concentration.

endoproteinase GluC (Roche Diagnostics, Australia) (10 ng/μL for 16 h at 37 °C).

MALDI-TOF Mass Spectrometry. Isolated peptides were identified by mass spectrometry using a Voyager-DE STR Perkin-Elmer Applied Biosystems matrix-assisted laser desorption/ionization time-of-flight (MALDI-TOF) spectrometer. HPLC samples were spotted in a 5:2 mixture of α-cyano-4-hydroxycinnamic acid in 50% acetonitrile and 1% TFA. Spectra were analyzed with MS-FIT and MS-Digest (*27*) (http://prospector.ucsf.edu/).

Purification of the KA−ApoC-II Adduct. Freshly prepared apoC-II (42 μM) was incubated for 3 h in the absence and presence of KA (100 μM) and then reduced with sodium borohydride (8.2 mM) for 30 min. Material corresponding to apoC-II linked to a single KA molecule, in addition to a control apoC-II sample, was isolated by HPLC and immediately dialyzed overnight against 10 mM ammonium bicarbonate. Dialyzed samples were then concentrated in a RVC 2-25 vacuum centrifuge (Christ, Germany) at 50 °C to a final concentration of 50 μM and incubated at 20 °C for 5 days before analysis by electron microscopy.

RESULTS

The chemical structures of KA and other derivatives used in this study are shown in Figure 1A. The influence of KA (60 μM) and other lipid metabolites on quiescent apoC-II amyloid fibril formation (42 μM) was examined at 37 °C by measuring the fluorescence of added ThT (Figure 1B). The ThT fluorescence profile for apoC-II alone (42 μM) showed a short lag phase (several hours), followed by a growth phase with maximum changes in fluorescence obtained after 60 h, with a half-time (t_{50}) of approximately

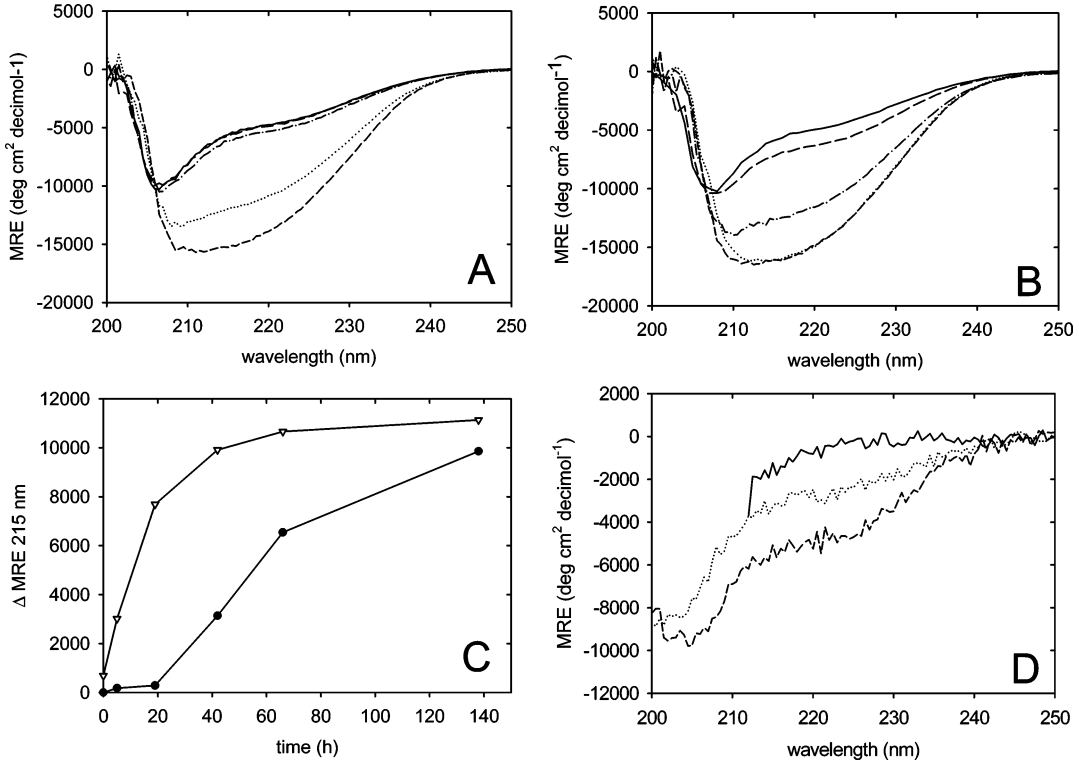

FIGURE 2: Effect of KA on apoC-II fibril formation monitored by CD spectroscopy. ApoC-II (42 μM) was incubated at 20 °C in the absence (A) and presence (B) of 60 μM KA at 0 h (solid line), 2 h (long dashed line), 22 h (dash-dotted line), 66 h (dotted line), and 138 h (short dashed line). (C) Changes in mean residue ellipticity (MRE) at 215 nm in the absence (closed circles) and presence (open triangles) of 60 μM KA. (D) CD spectra for apoC-II (11 μM) incubated for 30 min in 5 M GuHCl (solid line), apoC-II (11 μM) in 100 mM sodium phosphate, pH 7.4 (dotted line), or apoC-II (11 μM) with 60 mM KA in 100 mM sodium phosphate, pH 7.4 (dashed line). Spectra have been corrected for 5 M GuHCl alone, 100 mM sodium phosphate, pH 7.4, alone, or 60 μM KA in 100 mM sodium phosphate, pH 7.4, respectively.

23 h. Superstoichiometric amounts of KA (60 μM) caused an increase in the plateau value and a significant reduction in the t_{50} to approximately 4 h. However, equivalent concentrations of cholesterol or keto alcohol failed to significantly influence apoC-II fibrillogenesis. Other aldehyde-containing metabolites identified in atherosclerotic lesions, 4-hydroxy-2*E*-nonenal (4-HNE) and 9-oxononanoylcholesterol (9-ONC), at equivalent concentrations had no significant effect on the rate of apoC-II amyloid fibril formation, demonstrating the structural specificity of KA. The influence of KA on apoC-II fibril formation was also examined at lower temperature (20 °C; Figure 1C). Significant hastening was observed even at substoichiometric levels of KA. A plot of the t_{50} values versus the concentration of KA (Figure 1D) showed that KA rapidly reduced the half-time of apoC-II fibril formation over the concentration range of 0−40 μM, with further gradual changes at higher concentrations (60−150 μM). This concentration range is comparable to the range of cholesterol ozonolysis products detected in human atheroma, reported to be in the order of 10 pmol/mg (approximately 10 μM) in plaque material and up to 1.7 μM in plasma (*4*).

Amyloid fibril formation by apoC-II is accompanied by significant changes in secondary structure, as monitored by far-UV CD spectroscopy (*19*). The effect of KA on this process is shown in Figure 2. The progressive changes in CD spectra for apoC-II alone (42 μM) (Figure 2A) were significantly accelerated by the addition of KA (60 μM) (Figure 2B). Changes in ellipticity at 215 nm, reflecting increased β-sheet content, for apoC-II alone (Figure 2C) indicated a lag phase which was effectively abolished by the addition of KA. The half-time for change in MRE for apoC-II alone (approximately 60 h) was reduced to approximately 15 h in the presence of KA, comparable to the changes in the t_{50} values measured by ThT fluorescence in Figure 1D. To determine whether KA induced conformational changes in apoC-II that precede fibril formation, the CD spectra of freshly prepared apoC-II (11 μM) were measured in the absence and presence of KA (60 μM) (Figure 2D). Comparison of the CD spectra for apoC-II in 5 M GuHCl and in refolding buffer indicated a change in secondary structure in freshly refolded apoC-II. Adding KA to this freshly prepared apoC-II induced further changes in ellipticities, suggesting that KA alters apoC-II secondary structure. ThT fluorescence assays indicated that these changes in apoC-II secondary structure occurred before any significant fibril formation (data not shown).

We next determined the size distribution of the apoC-II fibrils by sedimentation velocity analysis (*28*) in the absence and presence of various concentrations of KA (Figure 3). ApoC-II fibrils (42 μM, 20 °C) formed over a period of 72 h without KA sedimented as a single uniform boundary (Figure 3A) with a significant amount of nonsedimenting absorbance corresponding to monomeric apoC-II. Fibrils formed in the presence of 20 or 100 μM KA (panels B and C of Figure 3, respectively) yielded similar sedimentation profiles with two notable differences. For the KA-containing samples there was a decrease in the nonsedimenting absorbance, corresponding to a reduction in the amount of monomeric apoC-II. This is consistent with the results

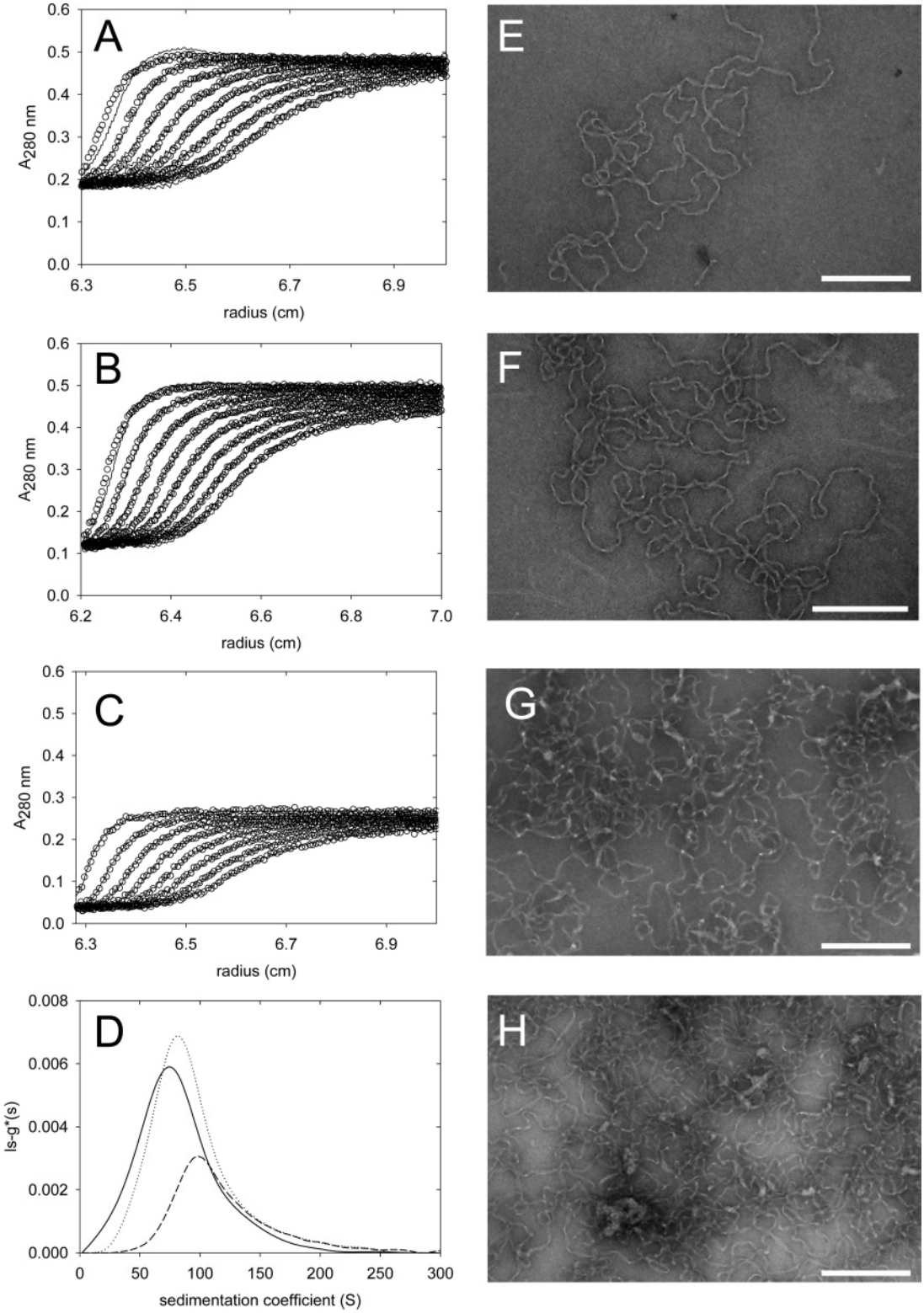

FIGURE 3: Effect of KA on apoC-II fibril formation monitored by sedimentation velocity and electron microscopy. Sedimentation velocity analysis of apoC-II fibrils (42 μM) formed for 72 h in the absence (A) and presence of 20 μM KA (B) or 100 μM KA (C). Ls-g*(s) sedimentation coefficient distributions for the data in panels A−C are given in panel D (solid line, dotted line, and dashed line, respectively). Electron micrographs of apoC-II fibrils grown in the absence (E) or presence (F) of 40 μM KA for 72 h. ApoC-II fibrils formed in the presence of 100 μM KA for 72 h were subjected to low-speed centrifugation (14000g, 30 min), and the supernatant and pellet fractions were examined by electron microscopy (panels G and H, respectively). Scale bars are 200 nm.

presented in Figures 1 and 2, which indicate that KA promotes apoC-II fibril formation. The second observation is that, for the apoC-II sample formed in the presence of 100 μM KA, there was a rapid loss of absorbance, due to very rapidly sedimenting material that disappeared prior to the first scan of the sample. This suggested substantial aggregation of apoC-II fibrils in the presence of high concentrations of KA. The data in Figure 3A−C were analyzed to obtain continuous sedimentation coefficient distributions (Figure 3D), which showed that apoC-II fibrils

formed in the presence and absence of KA had similar average sedimentation coefficients. The main difference was a reduction in the area under the curve for the apoC-II sample formed in the presence of 100 μM KA attributed to the loss of the very rapidly sedimenting high MW aggregates. When analyzed by electron microscopy, native apoC-II fibrils possessed a twisted ribbon morphology (Figure 3E) similar to that reported previously (*19*). ApoC-II fibrils formed in the presence of 40 μM KA showed similar fibril morphologies (Figure 3F) with no significant differences in twist repeat distance or fibril dimensions observed. The apoC-II sample formed in the presence of 100 μM KA was examined further by low-speed centrifugation (14000*g*, 30 min) to obtain pellet and supernatant fractions. Electron microscopy of the supernatant fraction (Figure 3G) showed typical twisted ribbon structures with adhering material suggesting bound aggregates of KA. For the pellet fraction (Figure 3H), the fibrils were more condensed and cross-linked with material putatively identified as KA aggregates.

Previous work has shown that KA forms Schiff base adducts with Aβ (1−40), forming spherical aggregates that initiate Aβ (1−40) fibril growth (*8*, *9*). If Schiff base formation is mechanistically important in accelerating fibrillogenesis, compounds that compete with the aldehyde of KA should inhibit the effect of KA. In the case of α-synuclein, amines fail to inhibit the KA activation of fibril formation, suggesting a noncovalent mechanism for KA activation (*10*). We examined the ability of several amine-containing compounds to inhibit KA-hastened apoC-II fibrillogenesis. Figure 4A shows the effect of lysine, bovine serum albumin (BSA), and apoA-I on the formation of apoC-II amyloid formation in the presence and absence of KA. Figure 4B shows similar experiments with L-carnosine and hydralazine. Lysine, BSA, and L-carnosine had no effect on the development of ThT fluorescence by apoC-II incubated for 7 h either in the presence or in the absence of KA. Of the amine-containing compounds tested, only hydralazine and apoA-I had any significant effect on the KA-induced acceleration of fibril formation by apoC-II. This suggests structural specificity in the ability of these amine-containing compounds to compete with apoC-II in the reaction with KA. We attribute the effect of apoA-I to the lipid-binding properties of apoA-I and consequent ability to sequester KA. To further probe the role of Schiff base formation between apoC-II and KA, we converted the aldehyde group of KA to an acid to prevent Schiff base formation. Converting the aldehyde group of KA to an acid incapable of Schiff base formation did not abolish the capacity to accelerate apoC-II fibril formation (Figure 4C). However, at equivalent concentrations, KA promoted apoC-II amyloid formation more effectively than the keto acid derivative.

The aldehyde functional group in KA appeared to be important for maximum acceleration of apoC-II fibril formation. Therefore, we investigated whether the addition of KA followed by borohydride reduction led to the formation of covalent KA adducts with apoC-II (Figure 5A). When analyzed by high-performance liquid chromatography (HPLC), freshly prepared apoC-II eluted at 35.5 min, with a predicted mass of 8914.9 determined by MALDI-TOF mass spectrometry. The sample of apoC-II refolded in the presence of KA and reduced with sodium borohydride showed a major peak at 35.5 min, coupled with additional minor peaks that eluted

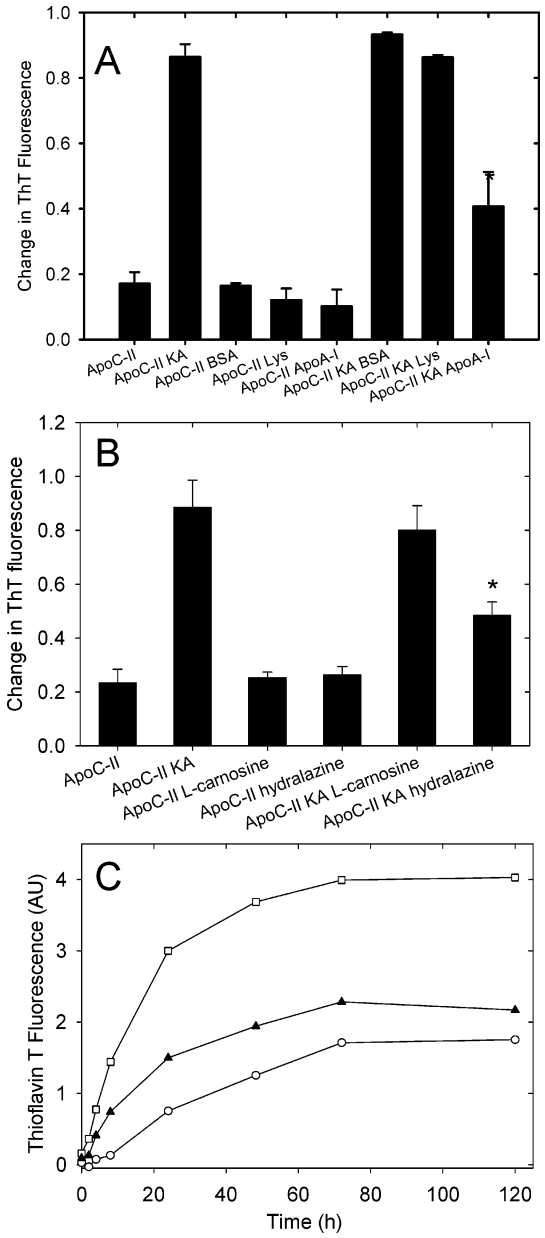

FIGURE 4: Effect of different amine derivatives and the keto acid derivative of KA on the acceleration of apoC-II fibril formation. (A) ApoC-II (42 μM) was incubated alone or in the presence of 60 μM KA, with or without various amine-containing compounds including BSA (100 μM), lysine (100 μM), and apoA-I (10 μM) at 20 °C. ThT fluorescence levels are shown after 7 h. The asterisk indicates statistically significant deviation ($P < 0.05$) compared to apoC-II and the KA sample. (B) ApoC-II (42 μM) was incubated alone or in the presence of 20 μM KA, with or without the amine-sequestering compounds L-carnosine (100 μM) and hydralazine (100 μM) at 20 °C. ThT fluorescence levels are shown after 7 h. The asterisk indicates statistically significant deviation ($P < 0.05$) compared to apoC-II and the KA sample. (C) ApoC-II (42 μM, open circles) was incubated with 60 μM KA (open squares) or the keto acid derivative (closed triangles) at 20 °C.

at 40 and 45 min. The masses of these minor populations were determined to be 9318.3 and 9720.6 Da. These masses are consistent with the addition of one and two molecules of KA (418.25 Da), respectively. Schiff base formation between the KA carbonyl group and the primary amine group of lysine results in the loss of a water molecule (−18), followed by the addition of two protons upon reduction with borohydride, leading to an overall mass difference between

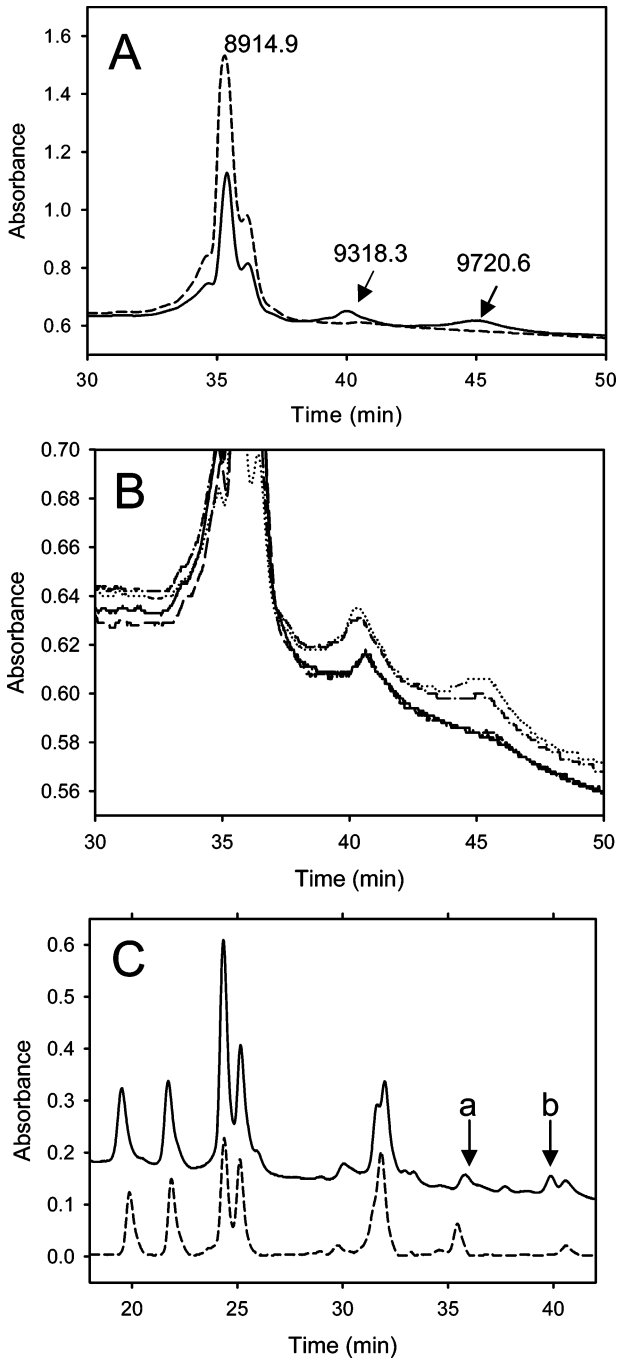

FIGURE 5: Characterization of KA-modified apoC-II. (A) ApoC-II monomers (42 μM) were incubated with KA (300 μM) at 20 °C for 3 h. Samples of native apoC-II (dashed line) and apoC-II incubated with KA (solid line) were reduced by the addition of 8 mM sodium borohydride and separated by high-performance liquid chromatography (HPLC). Masses of peaks as determined by mass spectrometry are shown in Da. (B) Effect of KA concentration on the formation of a Schiff base adduct with apoC-II. ApoC-II monomers (42 μM) were incubated with KA at various concentrations (20 μM, solid line; 100 μM, dashed line; 200 μM, dash-dotted line; 400 μM, dotted line) at 20 °C for 3 h. Samples were reduced by the addition of 8 mM sodium borohydride and separated by HPLC. (C) ApoC-II (dashed line) and KA-modified apoC-II (solid line) were treated with endoproteinase GluC for 15 h at 37 °C. Additional peaks present in apoC-II KA samples are labeled (a and b) and were identified by mass spectrometry (Table 1).

the reduced KA−apoC-II adduct and apoC-II of 402 per KA group. The presence of the apoC-II derivative with two KA molecules attached was concentration dependent (Figure 5B) and was only observed using concentrations of 200 and 400 μM KA, corresponding to a 5- and 10-fold molar excess of KA to apoC-II. We investigated the position of KA covalently linked to apoC-II within the apoC-II primary sequence. These experiments were performed using 100 μM KA incubated with 42 μM apoC-II, generating the KA−apoC-II derivative with a single KA molecule attached. Samples of both apoC-II and apoC-II incubated with KA and reduced by sodium borohydride were treated with endoproteinase GluC and analyzed by HPLC and MALDI-TOF mass spectrometry. The elution profile of GluC peptide fragments resulting from complete digestion of native apoC-II is shown in Figure 5C. The GluC digest elution profile of KA−apoC-II showed additional peaks caused by missed cleavages (labeled a and b), not present in the digestion profile of apoC-II alone. Peak b in Figure 5C contained two mass spectral peaks. Peaks a and b included peptides of masses 1598, 1780, and 4975 Da corresponding to apoC-II GluC peptides of residues 28−38, 9−20, and 39−79 with KA covalently attached (Table 1). Peaks a and b were reproducibly observed in several GluC digests. These data suggested modification of lysine residues 19, 30, 39, 48, 55, and 76, indicating no obvious preference for the modification of a particular residue. This heterogeneity of modification may account for other peaks observed in Figure 5C (for instance, between 36 and 39 min), which were not further analyzed. We did not determine whether the N-terminus is also modified by KA.

Table 1: Identification of Endoproteinase GluC Peptides from KA-Modified ApoC-II Using MALDI-TOF Mass Spectrometry[a]

peak	size of peptide determined by MS (*m/z*)	size (*m/z*) less KA (403 Da)	GluC peptide of apoC-II (residues)	lysine residue likely modified
a	1598	1195	28−38	30
b	1780	1377	9−20	19
b	4975	4572	39−79	39/48/55/76

[a] Peaks labeled in Figure 5C. ApoC-II amino acid sequence (lysine residues in bold): TQQPQQDEMP SPTFLTQV**K**E SLSSYWESA**K** TAAQNLYE**K**T YLPAVDE**K**LR DLYS**K**STAAM STYTGIFTDQ VLSVL**K**GEE.

We examined the ability of isolated KA−apoC-II adducts to form amyloid fibrils. To this end the KA−apoC-II adducts were purified, concentrated, and incubated for 5 days under quiescent conditions and then viewed by electron microscopy (Figure 6). A wild-type apoC-II control sample, purified under the same conditions, formed fibrils with a twisted ribbon morphology (Figure 6A) similar to the images shown in Figure 3E. In contrast, KA−apoC-II adduct polypeptides, containing no unmodified apoC-II, aggregated to form different morphologies, including amorphous aggregates of short fibrils (Figure 6B), simple short straight fibrils (Figure 6C), or highly ordered and branched straight fibrils (Figure 6D).

DISCUSSION

The results in Figures 1 (37 °C) and 2 (20 °C) show that KA accelerates apoC-II fibril formation, causing a significant reduction in the lag phase associated with amyloidogenesis. According to a simple nucleation elongation model, this suggests that KA acts via an increase in the rate of nucleation. While KA appears to hasten the rate of nucleation, nucleation

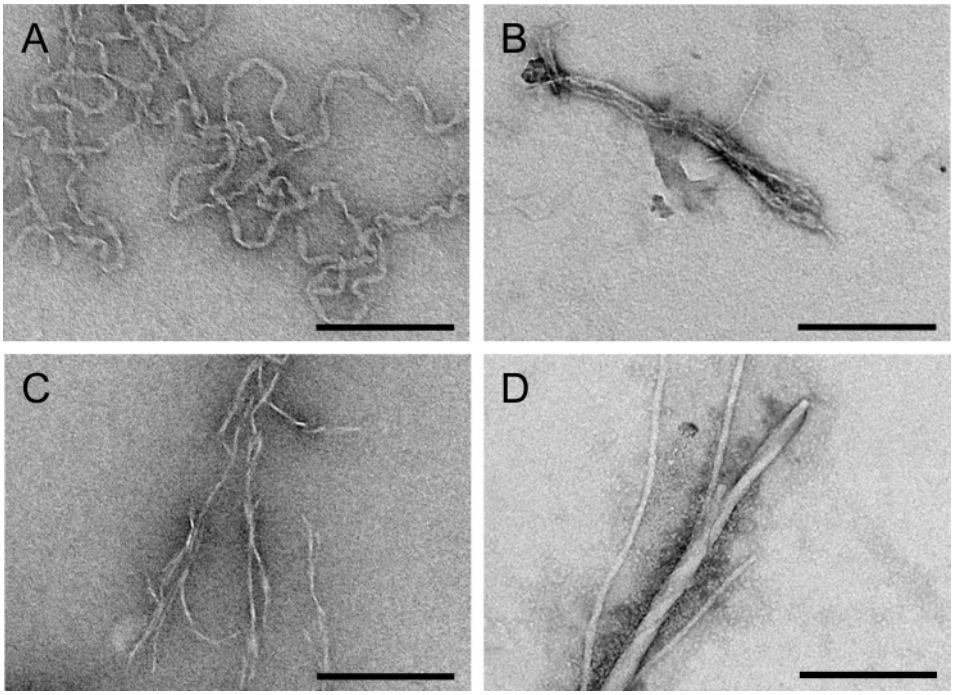

FIGURE 6: Transmission electron micrographs of apoC-II amyloid fibrils. Fibrils formed from apoC-II (A) and fibrils formed from the KA−apoC-II adduct (B−D). Scale bars are 200 nm.

theory predicts that an increase in the rate of nucleation should lead to an increase in fibril initiation and a reduction in the final average size of the fibrils (*29*). The size distribution of apoC-II fibrils formed in the presence of 20 μM KA is similar to those formed in the absence of KA, in contrast with these predictions (Figure 3). It is still possible that KA-hastened amyloidogenesis proceeds by a nucleated polymerization, with the final fibril length distribution determined by other factors, such as reversible subunit exchange and fibril breaking and joining, as demonstrated by recent results obtained with other amyloid systems (*30*). It is also possible that there is a change in mechanism to something approaching a downhill polymerization (*8*), wherein the introduction of KA-modified apoC-II molecules with unmodified apoC-II renders aggregation facile and thermodynamically favored for the initiating steps.

Circular dichroism data of freshly prepared apoC-II showed that KA induces changes in apoC-II secondary structure that precede fibril formation. These conformational changes occur under conditions where KA forms a covalent Schiff base with apoC-II (Figure 5). This Schiff base is critical to the KA-mediated acceleration of Aβ amyloid formation (*8*). However, the results in the present study suggest that there is also a noncovalent component to the effect of KA on apoC-II fibril formation since the keto acid derivative of KA retains partial ability to accelerate apoC-II fibril formation. Furthermore, competition experiments with several amine-containing compounds show structural specificity in the ability of these compounds to inhibit the effect of KA. We propose that the mechanism of acceleration by KA and the keto acid derivative involves a noncovalent interaction inducing a conformational change which is augmented, in the case of KA, by the formation of a Schiff base. According to this hypothesis this altered conformational state is more readily able to form fibrils. Fibril formation by Aβ, α-synuclein, and apoC-II, which are all lipid-binding proteins, is accelerated by KA, whereas the aggregation of transthyretin, a highly soluble amyloidogenic protein, is not promoted by KA (*9*). The ability of proteins to bind KA may be a requirement for the KA-mediated acceleration of their self-association into amyloid fibrils. Alternatively, it may be that natively unfolded proteins and conformationally fragile apoproteins are more susceptible to oxidative metabolite triggered misfolding because the influence on their physical properties is greater.

LDL oxidation has been widely studied as an initiation event in atherosclerosis. Our recent studies show that the oxidation of LDL generates amyloid-like structures that bind amyloid-specific dyes and acquire β-sheet structure (*31*). While the mechanism for the induction of amyloid-like properties in oxidized LDL has not been established, lipid modification and depletion may be contributing factors. For ozone-treated LDL particles, X-ray diffraction studies show the formation of cross-β-structure (*31*). We propose that conformational changes induced by KA, generated from cholesterol ozonolysis, may also play a role in the induction of conformational changes in apoB, the major protein constituent of LDL.

In addition to KA-induced changes in the conformation of apoC-II (Figure 2), KA also induces changes in Aβ (*8*) leading to the formation of fibrils with different morphologies. Aβ fibrils formed in the presence of KA have a longer repeat length and more complex morphology than those fibrils formed in the absence of KA (*8*). In contrast, fibrils formed by α-synuclein in the presence and absence of KA show no difference in morphology (*10*). Since the interaction of KA with α-synuclein is noncovalent, this may indicate that the covalent modification of Aβ and apoC-II by KA underlies the observed changes in morphology of these fibrils formed in the presence of KA.

There is a growing awareness that amyloid deposits are a common feature of atherosclerotic lesions. Recent studies have shown that amyloid is found in 54% of atherosclerotic intima (*13*) and that amyloid fibrils derived from apolipo-

proteins, β-amyloid, and SAA are present in atheroma (*32*, *33*). Apolipoproteins accumulate in the intima as a result of increased lipoprotein retention and/or macrophage secretion during hypercholesterolemic states. Full-length or truncated apoA-I, apoA-II, apoA-IV, apoC-II, and apoE have been shown to adopt amyloid structure both in vitro and in vivo (*17*). Aβ and apoC-II amyloid fibrils interact with macrophages in a CD36-dependent manner and induce inflammatory signaling cascades linked to inflammation and prothrombotic potential (*7*, *15*). The ability of KA to hasten apoC-II fibril formation suggests that a pool of oxidative intermediates may trigger or exacerbate amyloid deposition in vivo. This could lead to a vicious cycle wherein any inflammatory stress stimulus, such as an infection, could produce KA which triggers amyloidogenesis, causing more inflammation leading to higher concentrations of KA which further hastens apoC-II amyloidogenesis and proteotoxicity contributing to atherosclerotic disease. In addition, the capacity of KA to promote the formation of rapidly sedimenting material (Figure 3) and the ability of covalent KA adducts to generate fibrils with altered morphologies (Figure 6) may alter the properties of amyloid fibrils and the cellular responses in atherosclerosis. The ability of apoA-I and other lipid-binding proteins to sequester KA appears to inhibit the capacity of KA to induce amyloidogenesis, suggesting a potential therapeutic strategy.

REFERENCES

1. Lusis, A. J. (2000) Atherosclerosis, *Nature 407*, 233−241.
2. Libby, P. (2002) Inflammation in atherosclerosis, *Nature 420*, 868−874.
3. Bieschke, J., Zhang, Q., Bosco, D. A., Lerner, R. A., Powers, E. T., Wentworth, P., Jr., and Kelly, J. W. (2006) Small molecule oxidation products trigger disease-associated protein misfolding, *Acc. Chem. Res. 39*, 611−619.
4. Wentworth, P., Jr., Nieva, J., Takeuchi, C., Galve, R., Wentworth, A. D., Dilley, R. B., DeLaria, G. A., Saven, A., Babior, B. M., Janda, K. D., Eschenmoser, A., and Lerner, R. A. (2003) Evidence for ozone formation in human atherosclerotic arteries, *Science 302*, 1053−1056.
5. Babior, B. M., Takeuchi, C., Ruedi, J., Gutierrez, A., and Wentworth, P., Jr. (2003) Investigating antibody-catalyzed ozone generation by human neutrophils, *Proc. Natl. Acad. Sci. U.S.A. 100*, 3031−3034.
6. El, Khoury, J. B., Moore, K. J., Means, T. K., Leung, J., Terada, K., Toft, M., Freeman, M. W., and Luster, A. D. (2003) CD36 mediates the innate host response to beta-amyloid, *J. Exp. Med. 197*, 1657−1666.
7. Moore, K. J., El Khoury, J., Medeiros, L. A., Terada, K., Geula, C., Luster, A. D., and Freeman, M. W. (2002) A CD36-initiated signaling cascade mediates inflammatory effects of beta-amyloid, *J. Biol. Chem. 277*, 47373−47379.
8. Bieschke, J., Zhang, Q., Powers, E. T., Lerner, R. A., and Kelly, J. W. (2005) Oxidative metabolites accelerate Alzheimer's amyloidogenesis by a two-step mechanism, eliminating the requirement for nucleation, *Biochemistry 44*, 4977−4983.
9. Zhang, Q., Powers, E. T., Nieva, J., Huff, M. E., Dendle, M. A., Bieschke, J., Glabe, C. G., Eschenmoser, A., Wentworth, P., Jr., Lerner, R. A., and Kelly, J. W. (2004) Metabolite-initiated protein misfolding may trigger Alzheimer's disease, *Proc. Natl. Acad. Sci. U.S.A. 101*, 4752−4757.
10. Bosco, D. A., Fowler, D. M., Zhang, Q., Nieva, J., Powers, E. T., Wentworth, P., Lerner, R. A., and Kelly, J. W. (2006) Elevated levels of oxidized cholesterol metabolites in Lewy body disease brains accelerate alpha-synuclein fibrilization, *Nat. Chem. Biol.* (in press).
11. Mucchiano, G. I., Haggqvist, B., Sletten, K., and Westermark, P. (2001) Apolipoprotein A-1-derived amyloid in atherosclerotic plaques of the human aorta, *J. Pathol. 193*, 270−275.
12. Westermark, P., Mucchiano, G., Marthin, T., Johnson, K. H., and Sletten, K. (1995) Apolipoprotein A1-derived amyloid in human aortic atherosclerotic plaques, *Am. J. Pathol. 147*, 1186−1192.
13. Rocken, C., Tautenhahn, J., Buhling, F., Sachwitz, D., Vockler, S., Goette, A., and Burger, T. (2006) Prevalence and pathology of amyloid in atherosclerotic arteries, *Arterioscler., Thromb., Vasc. Biol. 26*, 676−677.
14. O'Brien, K. D., Olin, K. L., Alpers, C. E., Chiu, W., Ferguson, M., Hudkins, K., Wight, T. N., and Chait, A. (1998) Comparison of apolipoprotein and proteoglycan deposits in human coronary atherosclerotic plaques: colocalization of biglycan with apolipoproteins, *Circulation 98*, 519−527.
15. Medeiros, L. A., Khan, T., El, Khoury, J. B., Pham, C. L., Hatters, D. M., Howlett, G. J., Lopez, R., O'Brien, K. D., and Moore, K. J. (2004) Fibrillar amyloid protein present in atheroma activates CD36 signal transduction, *J. Biol. Chem. 279*, 10643−10648.
16. Mak, P. A., Laffitte, B. A., Desrumaux, C., Joseph, S. B., Curtiss, L. K., Mangelsdorf, D. J., Tontonoz, P., and Edwards, P. A. (2002) Regulated expression of the apolipoprotein E/C-I/C-IV/C-II gene cluster in murine and human macrophages. A critical role for nuclear liver X receptors alpha and beta, *J. Biol. Chem. 277*, 31900−31908.
17. Hatters, D. M., and Howlett, G. J. (2002) The structural basis for amyloid formation by plasma apolipoproteins: a review, *Eur. Biophys. J. 31*, 2−8.
18. MacRaild, C. A., Hatters, D. M., Howlett, G. J., and Gooley, P. R. (2001) NMR structure of human apolipoprotein C-II in the presence of sodium dodecyl sulfate, *Biochemistry 40*, 5414−5421.
19. Hatters, D. M., MacPhee, C. E., Lawrence, L. J., Sawyer, W. H., and Howlett, G. J. (2000) Human apolipoprotein C-II forms twisted amyloid ribbons and closed loops, *Biochemistry 39*, 8276−8283.
20. Powers, G. A., Pham, C. L., Pearce, M. C., Howlett, G. J., and Bottomley, S. P. (2007) Serpin acceleration of amyloid fibril formation: A role for accessory proteins, *J. Mol. Biol. 366*, 666−676.
21. MacRaild, C. A., Stewart, C. R., Mok, Y. F., Gunzburg, M. J., Perugini, M. A., Lawrence, L. J., Tirtaatmadja, V., Cooper-White, J. J., and Howlett, G. J. (2004) Non-fibrillar components of amyloid deposits mediate the self-association and tangling of amyloid fibrils, *J. Biol. Chem. 279*, 21038−21045.
22. Wilson, L. M., Mok, Y. F., Binger, K. J., Griffin, M. D., Mertens, H. D., Lin, F., Wade, J. D., Gooley, P. R., and Howlett, G. J. (2006) A structural core within apolipoprotein C-II amyloid fibrils identified using hydrogen exchange and proteolysis, *J. Mol. Biol.* (Dec 21; Epub ahead of print).
23. Lopez de la Paz, M., and Serrano, L. (2004) Sequence determinants of amyloid fibril formation, *Proc. Natl. Acad. Sci. U.S.A. 101*, 87−92.
24. Kawai, Y., Saito, A., Shibata, N., Kobayashi, M., Yamada, S., Osawa, T., and Uchida, K. (2003) Covalent binding of oxidized cholesteryl esters to protein: implications for oxidative modification of low density lipoprotein and atherosclerosis, *J. Biol. Chem. 278*, 21040−21049.
25. Hatters, D. M., Minton, A. P., and Howlett, G. J. (2002) Macromolecular crowding accelerates amyloid formation by human apolipoprotein C-II, *J. Biol. Chem. 277*, 7824−7830.
26. Schuck, P. (2000) Size-distribution analysis of macromolecules by sedimentation velocity ultracentrifugation and lamm equation modeling, *Biophys. J. 78*, 1606−1619.
27. Clauser, K. R., Baker, P., and Burlingame, A. L. (1999) Role of accurate mass measurement (±10 ppm) in protein identification strategies employing MS or MS/MS and database searching, *Anal. Chem. 71*, 2871−2882.
28. MacRaild, C. A., Hatters, D. M., Lawrence, L. J., and Howlett, G. J. (2003) Sedimentation velocity analysis of flexible macromolecules: self-association and tangling of amyloid fibrils, *Biophys. J. 84*, 2562−2569.
29. Come, J. H., Fraser, P. E., and Lansbury, P. T., Jr. (1993) A kinetic model for amyloid formation in the prion diseases: importance of seeding, *Proc. Natl. Acad. Sci. U.S.A. 90*, 5959−5963.
30. Carulla, N., Caddy, G. L., Hall, D. R., Zurdo, J., Gairi, M., Feliz, M., Giralt, E., Robinson, C. V., and Dobson, C. M. (2005) Molecular recycling within amyloid fibrils, *Nature 436*, 554−558.

31. Stewart, C. R., Tseng, A. A., Mok, Y. F., Staples, M. K., Schiesser, C. H., Lawrence, L. J., Varghese, J. N., Moore, K. J., and Howlett, G. J. (2005) Oxidation of low-density lipoproteins induces amyloid-like structures that are recognized by macrophages, *Biochemistry 44*, 9108−9116.
32. Howlett, G. J., and Moore, K. J. (2006) Untangling the role of amyloid in atherosclerosis, *Curr. Opin. Lipidol. 17*, 541−547.
33. O'Brien, K. D., McDonald, T. O., Kunjathoor, V., Eng, K., Knopp, E. A., Lewis, K., Lopez, R., Kirk, E. A., Chait, A., Wight, T. N., deBeer, F. C., and LeBoeuf, R. C. (2005) Serum amyloid A and lipoprotein retention in murine models of atherosclerosis, *Arterioscler., Thromb., Vasc. Biol. 25*, 785−790.

BI602554Z